Fabry–Pérot nanocavities in multilayered plasmonic crystals for enhanced biosensing

Alp Artar, Ahmet Ali Yanik, and Hatice Altug[a)]
Department of Electrical and Computer Engineering and Boston University Photonics Center, Boston University, Boston, Massachusetts 02215, USA

(Received 8 May 2009; accepted 15 July 2009; published online 6 August 2009)

We have demonstrated extraordinary light transmission effect through Fabry–Pérot cavities in multilayered plasmonic crystals formed by coupling two physically separated metallic nanohole and nanodisk array layers. Superior field-medium overlap is observed with Fabry–Pérot resonances as a result of stronger electromagnetic field confinement in the dielectric region far from the metallic surfaces. We show that these cavity resonances are highly sensitive to refractive index changes. The large field-material overlap combined with simple fabrication scheme used here makes these structures an ideal candidate for biosensing applications. © *2009 American Institute of Physics*. [DOI: 10.1063/1.3202391]

The ability to confine electromagnetic waves on metallic surfaces in the form of localized and propagating surface plasmons (SPP) has opened up possibilities reshaping the photonics field.[1,2] By increasing the light-matter interactions, orders of magnitude enhancements in nonlinear phenomena such as second harmonic generation, fluorescence, and surface enhanced Raman scattering have been demonstrated.[3–5] Orders of magnitude stronger transmission through the subwavelength nanoapertures are shown in contrast to the prediction of the classical aperture theory of Bethe.[6,7] Unprecedented electromagnetic properties otherwise not possible in nature are observed in artificial crystals of metaatoms.[8] So far, studies are focused on two-dimensional (2D) arrangement of plasmonic nanostructures. However, engineering of materials in three dimensions (3D) by integrating different kinds of plasmonic resonances in multilayers offers additional degrees of freedom in our design space.[9,10]

In this letter, we demonstrate extraordinary light transmission effect in multilayered plasmonic crystals formed by coupling of two physically separated metal nanohole and nanodisk array layers (Fig. 1). We demonstrate that this multilayered plasmonic structures support Fabry–Pérot (FP) resonances in addition to the grating based SPP modes of conventional nanohole arrays with optical transmission efficiencies greater than predicted by Bethe's theory. We introduce a cavity model to explain the experimentally measured transmission spectra of the FP modes. The transmission strength of the FP resonances is observed to be strongly affected by their spectral overlap with the SPP modes. Electromagnetic fields of these FP resonances are confined in the dielectric region instead of the metallic surfaces enabling superior field-medium overlap. As a result, we show that they are highly sensitive to the refractive index (RI) changes within the media. The large field-medium overlap makes these structures an ideal candidate for biosensing applications. Furthermore, simplicity of the fabrication scheme used here conveniently eliminates the use of more specialized focused ion beam tool and enables nanohole array fabrication in a single step with more widely available e-beam lithography (EBL).

The schematic and the scanning electron microscope image of a fabricated multilayered plasmonic crystal are shown in Fig. 1. The structure consists of two physically separated plasmonic layers: the top one is a 2D nanohole array and the bottom one is a 2D array of gold nanodisks embedded in polymethyl methacrylate (PMMA) ($n=1.46$). These layers are fabricated on indium tin oxide glass substrate with a single EBL step and a highly directional e-beam metal deposition. Here, the 100 nm thick gold layer is deposited on a thin adhesion layer of 5 nm Ti. In the following measurements, the thickness of the dielectric layer (PMMA) is 350 nm unless otherwise is stated.

Zero-order transmission spectra obtained at normal incidence exhibit strong wavelength dependence as a result of complex interplay of diffraction, interference, and plasmonic resonances.[11,12] Figure 2(b) shows the transmission spectra of the arrays with 300 nm hole diameter for varying periodicities from 400 to 550 nm with increments of 50 nm. Absolute transmissions are calculated by normalizing the transmitted light intensity with the incident light. Signal strengths of the observed peaks are higher than the predicted values by Bethe's theory, confirming the extraordinary nature of the transmission phenomena. We observed that the position of certain transmission resonances depend on the lattice constant as in conventional nanohole arrays with the following formula:

$$\lambda_{\max} = \frac{p}{\sqrt{i^2 + j^2}} \sqrt{\frac{\varepsilon_d \varepsilon_m}{\varepsilon_d + \varepsilon_m}}, \tag{1}$$

where ε_d and ε_m are the dielectric constant of the medium and metal, p is the periodicity, and (i,j) are the grating or-

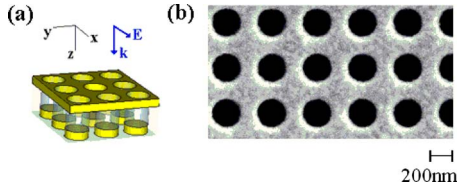

FIG. 1. (Color online) (a) Schematics of the multilayered plasmonic crystals; blue arrows show incident light configuration. (b) SEM image of a periodic array (diameter=250 nm and period=400 nm).

[a)]Electronic mail: altug@bu.edu.

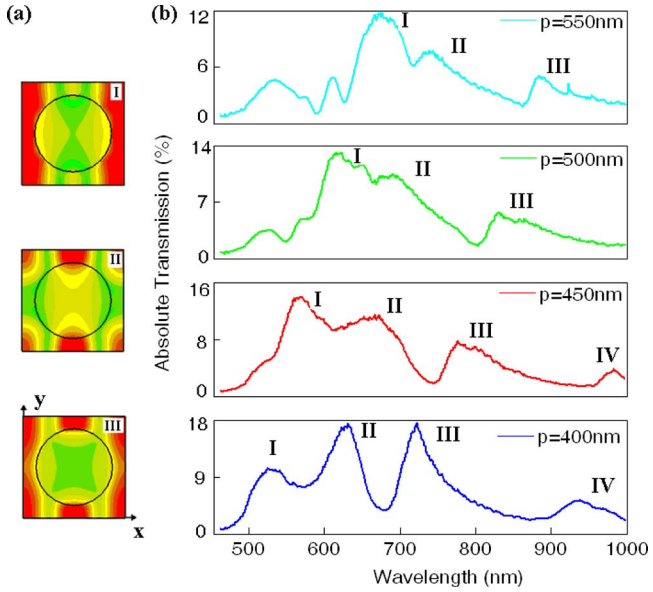

FIG. 2. (Color online) (a) H_y field patterns of $(1,0)_{\mathrm{Au/air}}$, $(1,1)_{\mathrm{Au/PMMA}}$, and $(1,0)_{\mathrm{Au/PMMA}}$ are shown, respectively, from top to down. (b) The absolute transmission spectra of the structures for crystals with diameter (d =300 nm) and varying periodicities (p) from 550 to 400 nm with 50 nm steps, respectively, from top to down.

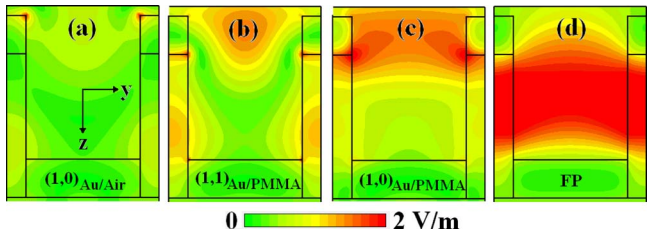

FIG. 3. (Color online) Cross sectional E_x field patterns are shown for (a) $(1,0)_{\mathrm{Au/air}}$, (b) $(1,1)_{\mathrm{Au/PMMA}}$, (c) $(1,0)_{\mathrm{Au/PMMA}}$, and (d) FP peaks. Cross sections are obtained at resonance peaks (f_a=575 THz, f_b=505 THz, f_c =434 THz, and f_d=320 THz, respectively) using a Fourier transform. Simulation is done with a structure of 300 nm diameter and 400 nm periodicity.

ders. At this wavelength, the Bragg condition is satisfied with the set of reciprocal lattice vectors $\vec{G}=i\vec{G}_x+j\vec{G}_y$ labeled by the integers (i,j). As shown in Fig. 2(b), experimentally measured (1,0) resonance for the gold/air interface and the (1,0), (1,1) resonances for the gold/PMMA interface are obtained, in good agreement with the analytical predictions given in Eq. (1).

To further clarify the observed resonances, we obtained the near field mode profiles by 3D finite-difference time-domain (FDTD).[13] Here, a linearly polarized pulsed plane wave excitation (with amplitude of 1 V/m) illuminates the device from the air side at normal incidence. Spectral responses are obtained in the far-field for the transmitted light. Resonance frequencies determined from the spectral response are used to map the field profiles using frequency monitors. For x-polarized incident light from the air side where z is the propagation direction, the dominant magnetic field profiles in y-direction are shown in Fig. 2(a) at transmission resonances for $(1,0)_{\mathrm{Au/Air}}$, $(1,1)_{\mathrm{Au/PMMA}}$, and $(1,0)_{\mathrm{Au/PMMA}}$, respectively. A symmetric standing wave pattern is evident in all spatial profiles as a result of two counterpropagating SPPs created at the related transmission maxima. For the resonance orders with (1,0) for both Au/Air and Au/PMMA interfaces, interference of counterpropagating standing wave pattern creates a cosine pattern. On the other hand, for $(1,1)_{\mathrm{Au/PMMA}}$ resonance the spatial pattern reflects a diagonal standing wave pattern with respect to basic lattice vectors of the rectangular lattice [Fig. 2(a)]. In addition, hot spots due to the localized surface plasmon (LSP) excitation at the rims of the apertures are discernible with strong resemblance to magnetic dipole excitations (reflecting the hybrid nature of the transmission resonances). Cross sectional field profiles obtained by 3D FDTD simulations for different resonances are shown in Fig. 3. Plasmonic excitations for $(1,0)_{\mathrm{Au/air}}$ mode is clearly confined at the air interface, and the strongest field densities are found around the nanohole rims as shown in Fig. 3(a). For the $(1,0)_{\mathrm{Au/PMMA}}$ and $(1,1)_{\mathrm{Au/PMMA}}$ resonances, the electric fields are confined at the Au/PMMA interface. Since light can only access the Au/PMMA grating modes through the LSPs excited at the air interface, the field lines are observable in the nanohole openings.

In transmission spectra shown in Fig. 2(b) (as well as in FDTD simulations), we observed a fourth transmission peak, which cannot be associated with any of the SPP based grating orders. According to our FDTD results [Fig. 3(d)], the upper surface of the gold nanodisks in the bottom interface and the bottom surfaces of the nanoholes on the top interface create a resonant cavity with strong field confinement. As a result, we called this resonance as FP mode. The field profile of the FP mode has been found to be coupled in the lateral direction and well confined in the z-direction with strong concentration in the dielectric region.

In contrast to SPPs, experimental measurements show that the spectral location of the FP nanocavity resonances is both controlled by the physical separation between the nanostructured layers and by the dimension and the periodicity of the holes. We can explain this behavior using a simple cavity model. The governing formula for the fundamental FP peak wavelength is $\lambda_{\mathrm{FP}}=2dn_{\mathrm{eff}}$, where d is the distance between the two confining layers and n_{eff} is the effective RI. As shown in Fig. 3(d), the field is confined nearly equally in the air and the PMMA layer, therefore enabling us to crudely model the effective RI as a weighted average of the RIs of the dielectrics in proportion with their volumes. Transmission spectra shown in Fig. 4 support the model.

As shown in Fig. 4(a), for an increase in PMMA thickness from 300 nm (blue curve) to 350 nm (red curve) at a fixed periodicity and hole/disk size, SPP plasmonic resonances are negligibly affected, while the FP excitation peak redshifts significantly (about 150 nm). This observation shows that FP resonance is strongly influenced by the spacing between the plasmonic nanostructured layers. Similarly, increasing hole/disk diameter at a fixed periodicity and layer separation does not affect the grating orders but blueshifts the FP peak [Fig. 4(b)] as a result of decreasing effective RI. On the other hand, increasing periodicity results in a redshifting of both the FP and the grating based SPP modes [Fig. 4(c)]. The redshifting of the FP can be accounted for an increase in n_{eff}, while the redshifting of the SPP modes can be explained by Eq. (1).

Due to the subwavelength dimensions of the nanoholes, normally incident collimated light cannot directly access into the FP cavity. The scattering from the periodic nanohole arrays and the associated SPPs on the metal/dielectric interface

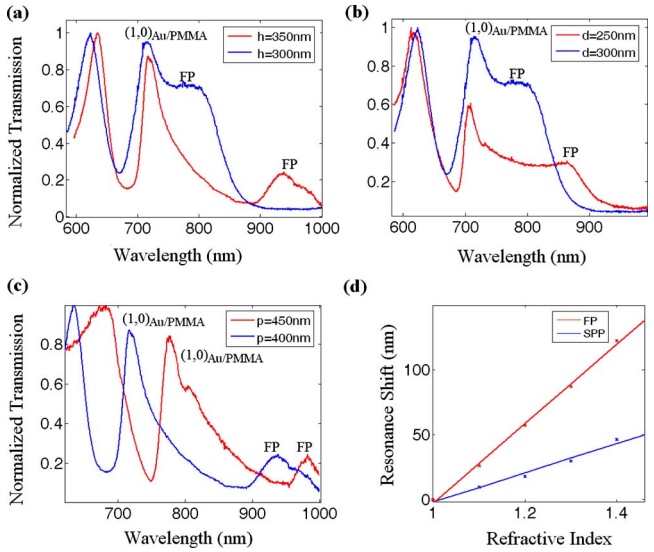

FIG. 4. (Color online) Comparison of spectrum (a) with changing dielectric layer thickness, (b) with changing diameter, and (c) with changing periodicity. (d) Shifts in spectral position with changing RI for FP peak (red) and $(1,0)_{\mathrm{Au/PMMA}}$ peak (blue).

offer a path for coupling. As shown in Fig. 4(a), we experimentally observe that the transmission efficiency of FP mode increases when it spectrally gets closer to the $(1,0)_{\mathrm{Au/PMMA}}$ order as a result of decreasing layer separation. A similar trend is also observed in measurements shown in Fig. 4(b). A decrease in radius spectrally moves FP peak away from the $(1,0)_{\mathrm{Au/PMMA}}$ order and results in a sharp drop in its transmission efficiency. On the other hand, increasing periodicity has minimal effect on the strength of the FP mediated transmissions since the spectral locations of the SPP and the FP redshift together.

What makes this fundamental FP mode more interesting is its potential for possible applications in bio/chemical sensing. As discussed above, the cross sectional field pattern of this peak is markedly different from those of the SPP resonances and shows stronger field concentration in the dielectric medium, as opposed to the metallic surfaces. Accordingly, a larger portion of the resonant excitation is exposed to the RI changes in the medium. Figure 4(d) shows the spectral shift in the FP (red line) and SPP (blue line) resonances as a function of bulk RI of the medium. According to our FDTD simulations, FP resonance is nearly three times more sensitive to the RI changes than the SPP resonances, 305 nm/RIU versus 110 nm/RIU (where RIU stands for refractive index unit).

In conclusion, we have shown extraordinary transmission effect through FP resonances in multilayered plasmonic crystals consisting of two coupled plasmonic nanostructured layers. To confirm the presence of the FP resonances, we have presented FDTD analysis. We introduced an analytical cavity model based on the effective RI approximation to explain the responses of FP modes in the spectral measurements. We showed that this multilayered structure also supports grating based SPP modes as in the conventional nanohole arrays. The spectral overlap of the SPP and FP modes has been observed to be strongly affecting the transmission strength of the FP resonances. Larger sensitivities to the RI changes in the medium for the nanocavity resonances are shown, an effect we attribute to strong field confinement in the dielectric media. The large field-material overlap combined with simplicity of the fabrication scheme used here makes these structures an ideal candidate for biosensing, as well as other applications in plasmonics.

This work is partly supported by SGER Program of NSF (Grant No. ECCS-0849603, directed by Eric Johnson), NSF funded Engineering Research Center on Smart Lighting, Massachusetts Life Science Center, Army Research Laboratory, Boston University Photonics Center, and Boston University College of Engineering for Dean's Catalyst Award.

[1] C. Genet and T. W. Ebbesen, Nature (London) **445**, 39 (2007).
[2] E. Ozbay, Science **311**, 189 (2006).
[3] S. Kim, J. Jin, Y. J. Kim, I. Y. Park, Y. Kim, and S. W. Kim, Nature (London) **453**, 757 (2008).
[4] Y. Liu and S. Blair, Opt. Lett. **28**, 507 (2003).
[5] S. Nie and S. R. Emory, Science **275**, 1102 (1997).
[6] T. W. Ebbesen, H. J. Lezec, H. F. Ghaemi, T. Thio, and P. A. Wolff, Nature (London) **391**, 667 (1998).
[7] A. A. Yanik, X. Wang, S. Erramilli, M. K. Hong, and H. Altug, Appl. Phys. Lett. **93**, 081104 (2008).
[8] J. B. Pendry, Phys. Rev. Lett. **85**, 3966 (2000).
[9] E. M. Hicks, X. Zhang, S. Zou, O. Lyandres, K. G. Spears, G. C. Schatz, and R. P. Van Duyne, J. Phys. Chem. B **109**, 22351 (2005).
[10] M. E. Stewart, N. H. Mack, V. Malyarchuk, J. A. N. T. Soares, T.-W. Lee, S. K. Gray, R. G. Nuzzo, and J. A. Rogers, Proc. Natl. Acad. Sci. U.S.A. **103**, 17143 (2006).
[11] P. B. Catrysse and S. Fan, J. Nanophotonics **2**, 021790 (2008).
[12] E. Ekinci, H. H. Solak, and C. David, Opt. Lett. **32**, 172 (2007).
[13] Microwave Studio is a registered trademark of CST GmbH, Darmstadt, Germany.